Charge-Density Analysis at the Turn of the Century

Philip Coppens

Chemistry Department, State University of New York at Buffalo, Buffalo, New York 14260-3000, USA.
E-mail: coppens@acsu.buffalo.edu

Abstract

X-ray diffraction is now used in an increasingly routine fashion for the measurement of charge densities in solids. The development of the method over the past decades is described briefly. The course of a modern charge-density analysis is outlined and the features of the aspherical atoms used in such an analysis are described. In addition to representing the detailed charge distribution, the results can be used to derive electrostatic moments of molecules and *d*-orbital populations of transition-metal atoms. Topological analysis of the experimental density yields quite reproducible results when related molecules are compared, but differences with Hartree–Fock theory remain, in particular for more polar bonds. For transition-metal complexes, patterns revealing the nature of the metal–ligand interaction are becoming apparent. The analysis of intermolecular interactions from the experimental density is developing rapidly.

1. Background

As the X-ray scattering of electrons is much stronger than that of the nuclei, the intensities of scattered X-rays are dominated by the distribution of the electrons. Therefore, with the exception of a few highly specialized experiments in which the nuclear scattering is measured, X-ray diffraction gives information on the electron distribution in the crystal. Conventional structure determination relies on the strong attraction between the electrons and the nuclei, which is the reason that the maxima in the electron density tend to coincide with the nuclear positions. This is a reasonable assumption, valid to a very good approximation, except for H atoms, which lack a core shell of electrons. As early as the 1950s, it was recognized that the anomalously short $X-$H bond lengths from X-ray diffraction were due to the migration of density from the nuclear region of the H atom into the $X-$H bond. A less-accurate assumption of conventional structure analysis, used in least-squares refinements, is that the atoms in a crystal each have the electron density of a spherically averaged isolated ground-state atom. This is of course incorrect. It is the aim of X-ray charge-density analysis to map the electron distribution in crystals and analyze all the detail that carries the information on chemical bonding.

The potential for measurement of the experimental charge distribution in crystals by X-ray diffraction did not escape the attention of the early pioneers of X-ray diffraction. But the measurement techniques of the 1920s and early 1930s were far too crude to show any deviations from spherical atomic distributions. Later efforts were concentrated on simple ionic compounds such as NaCl and MgO, for which deviations from spherical symmetry are very small. Thus, the measurement of charge densities remained a distant and mostly unachievable goal for decades, even though attempts were not lacking. But a much more advanced technology than that available at the time was needed.

Technical developments that occurred in the 1960s and 1970s include the design of new diffractometers, automation of data collection, much better low-temperature techniques, neutron diffraction and advances in computing power and software. Neutron diffraction provided an independent source of positional and thermal parameters, unbiased by the isolated-atom assumptions. Most of the analyses in this period were based on the *deformation electron density* (DED), defined as the difference between the observed density and that of a superposition of spherical atoms, or promolecule. An example showing the bending of the bonds in the cyclobutadiene ring is shown in Fig. 1.

When neutron parameters were used in the calculation of the DED, bonding features, which in least-squares analysis of X-ray data were masked by adjustments of the parameters, became readily apparent. This '$X-N$' technique was quickly complemented by '$X-X$'

Philip Coppens received his doctorate in Chemistry in 1960 from the University of Amsterdam with Professor Carolyn MacGillavry, based on work done at the Weizmann Institute of Science. He has worked at Brookhaven National Laboratory, and at present carries the rank of Distinguished Professor of Chemistry at the State University of New York at Buffalo. His research interests include X-ray charge analysis, chemical applications of synchrotron-radiation crystallography and the study of photoinduced states in molecular crystals. He is a past President of the International Union of Crystallography.

methods, in which less-biased parameters from high-order refinement of the X-ray data were used in the calculation of the promolecule density. The results were dramatic as they showed for the first time density-based experimental evidence for overlap between atomic orbitals, lone pairs, the bending of bonds in strained-ring systems and π bonding. These advances in X-ray charge-density analysis were achieved through a broad international effort, with major contributions from scientists in Australia, Denmark, Finland, France, Germany, Israel, Italy, Japan, the Netherlands, Russia, Sweden, Taiwan, the UK, the USA and elsewhere.

The developments of the 1960s are now complemented by the advent of area detectors, the availability of synchrotron radiation, abundant and cheap computing power, and by the development of program systems specifically designed for charge-density analysis. A recent report describes how the charge density of DL-proline was obtained in one day of experimentation at a synchrotron source (Koritsanszky *et al.*, 1998). This is comparable to the time needed for a theoretical calculation. It suggests that an 'electron-density microscope', which would allow on-line examination of the electron density in a crystal, may be achievable in the coming years.

2. Elements of a modern charge-density study

Given the proper equipment and some experience, a typical charge-density study can now be performed in a few days or less, provided a good-quality crystal is available. Data can be collected with an area detector, using the oscillation method. The crystal is rotated through a succession of small ranges. In each range, the intensities of the scattered beams are recorded and read out from the detection device. While not necessarily more accurate than measurements obtained with a point detector, *i.e.* a scintillation counter, area-detector data sets commonly have a large redundancy. This means that after suitable averaging of multiply measured and symmetry-equivalent reflections more reliable structure-factor amplitudes are obtained. For many studies, Mo $K\alpha$ radiation ($\lambda = 0.7107$ Å) is quite adequate, however there are advantages to collecting data at the shorter wavelengths and bright beams now available at many synchrotron sources. Cooling of the crystal to liquid-nitrogen temperature is usually essential. An appreciable additional gain is achieved by cooling to liquid-helium temperature, at which thermal smearing and especially anharmonic thermal effects are much reduced (Destro *et al.*, 1989; Larsen, 1995; Iversen *et al.*, 1996, 1997).

After application of standard well understood intensity corrections, followed by structure determination if the structure is not known, a least-squares refinement with aspherical atomic density functions is carried out. The exact choice of the density functions, and their

number, depends on the extent of the data set and the problem to be addressed, as discussed further below. The analysis of the charge density is now largely based on the 'model' electron densities that can be plotted with the least-squares parameters and corresponding functions. Electrostatic interactions between molecules in a crystal can be calculated from the least-squares results and so can *d*-orbital populations of transition-metal compounds.

In the last few years, the theory of *atoms in molecules* (AIM) of Bader and co-workers (Bader, 1990) has proven to be a powerful method for relating features of the charge density, experimental or theoretical, to chemical concepts. The AIM analysis is based on the topological features of the total density, such as its critical points, the density and Laplacian of the density ($\nabla^2 \rho$) at the critical points. As the theory is fully based on the electron density, it is very well suited for use in an experimental charge-density analysis. The experimental electron density can be obtained simply by Fourier transform of the structure-factor amplitudes, provided the phases are known. But such a density is not suitable for topological analysis, because even small experimental noise will create local maxima and minima, *i.e.* critical points, which dominate the topology. Series termination, owing to the finite resolution of the experimental data, has the same effect. Furthermore, the higher derivatives of the electron density, such as the Laplacian, are increasingly dependent on the high-order data. On the other hand, the density represented by the least-squares model functions does not suffer from such drawbacks because the density functions used in the
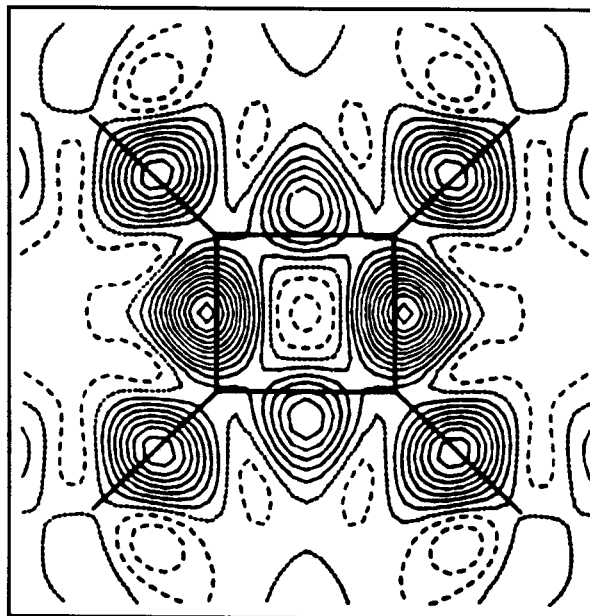

Fig. 1. Deformation density in a section through the cyclobutadiene ring determined at 110 K. Contours at 0.05 e Å^{-3}. Negative contours broken, zero contour dotted (Irngartinger, 1982).

algorithm are smoothly varying. Provided the functions used provide a proper description and fill the space in the crystal adequately, the model density provides the necessary starting point for the topological analysis.

3. The aspherical-atom least-squares analysis

Using aspherical atoms to describe the charge density in a bonded system is fully compatible with chemical bonding theory, which tells us that bonding is directional, and that lone-pair orbitals occur with double occupancy. But the aspherical-atom formalism does not explicitly account for the overlap density in a covalent bond between atoms, represented by two-center terms in the charge density calculated by theory. This is less of a limitation than may be expected, as directional atom-centered functions are sufficiently diffuse to account for the bonding density also. Thus, the atom-centered functions also represent the two-center overlap density between atoms. Because of this, Stewart introduced the term *pseudo-atom* to describe the sum of the atom-centered densities (Stewart, 1976).

The algorithm expresses the atomic density as an expansion of spherical harmonic functions centered on the nucleus. In the Hansen & Coppens (1978) formulation, the pseudo-atom density is defined as

$$\rho_{at}(\mathbf{r}) = P_c \rho_{core}(r) + P_v \kappa^3 \rho_{valence}(\kappa r)$$
$$+ \sum_{l=0}^{l_{max}} \kappa'^3 R_l(\kappa' r) \sum_{m=0}^{l} P_{lm\pm} d_{lm\pm}(\theta, \varphi). \quad (1)$$

The populations P_v, $P_{lm\pm}$ and radial expansion/contraction parameters κ and κ' are treated as *charge-density variables* in the least-squares refinement with aspherical form factors corresponding to the atoms defined by (1). Such charge-density variables are added to the positional and thermal parameters, which are refined in conventional structure determination. The core population P_c is usually kept fixed at the filled-shell value. Slater-type exponential functions are frequently used for the radial functions R_l. The angular functions $d_{lm\pm}$ are real spherical harmonic functions and thus identical in shape to the atomic orbitals used in quantum chemistry. However, in charge-density analysis they describe the density distribution rather than the wave function.

Since atoms vary in electronegativity, the parameter P_v will generally not be that of the neutral atom. But the crystal as a whole is neutral. This condition is commonly introduced as a constraint in the refinement. The change in the atomic electron population affects the electron–electron repulsion and therefore the radial dependence of the charge density centered on an atom. This is the reason for the introduction of the 'expansion/contraction' parameters κ and κ' (Coppens *et al.*, 1979), which multiply the radial coordinate. When κ is larger than one, the same density occurs at smaller r, thus the atom

is contracted relative to the functions introduced at the beginning of the refinement. A change in κ' also allows for the fact that the atom-centered functions must represent the density in the more distant bonding regions. Thus, relative to the spherical isolated atom, κ' will often be smaller than one.

The refined parameters, together with the density functions to which they refer, provide an analytical description of the electronic charge density. In principle, this is a description of the static density, as the effect of the thermal smearing of the density is separately accounted for by the temperature factors in the scattering formalism. Thus, within the limitations of that formalism, the thermal motion has been deconvoluted from the density. An example of a model-based deformation density is shown in Fig. 2.

The populations and shape of the atom-centered spherical harmonic density functions in (1) are directly related to the electrostatic atomic moments. The total valence charge follows from the $l = 0$ monopolar function, the atomic dipole moments from the three dipolar functions with $l = 1$, the quadrupole moments from the functions with $l = 2$ *etc*. It is often sufficient to truncate the expansion at the $l = 3$, octupolar, level for light atoms and at the $l = 4$, hexadecapolar, level for transition-metal atoms in molecular complexes. In extended solids with atoms located at highly symmetric sites, spherical harmonic functions with higher indices may be needed.

One measure of the success of the aspherical-atom refinement is provided by the rigid-bond test, first
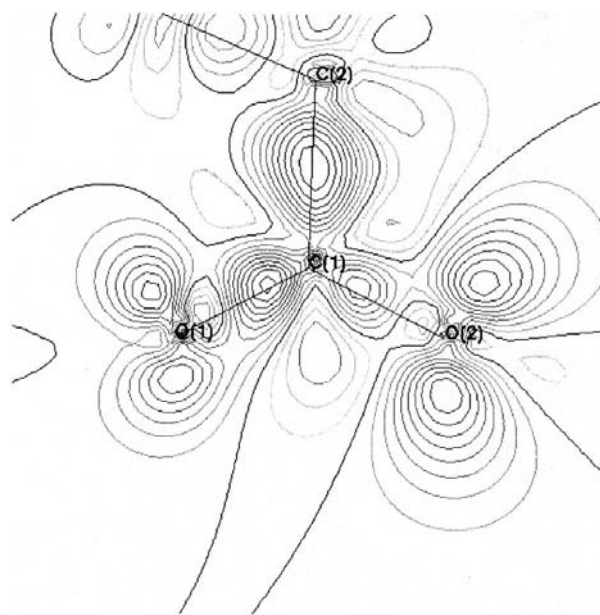

Fig. 2. Model based on deformation density in the COO plane in a crystal of DL-histidine. Contours at 0.1 e Å^{-3}. Heavy lines: positive and zero contours. Light lines: negative contours (Coppens *et al.*, 1998).

applied by Hirshfeld (1976). It stipulates that the mean-square amplitudes of vibration of the two atoms forming a covalent bond should be essentially equal, with a difference of less than 0.0010 Å^2 along that bond. It is found that the condition is much more closely obeyed when the aspherical-atom formalism is used, attesting to the validity of the aspherical-atom treatment. But some differences remain, as the atoms may have different amplitudes under the internal modes of a molecule. A further difficulty is the treatment of the H atoms. As the H atom lacks core electrons, it is not possible to refine simultaneously anisotropic thermal parameters and charge-density parameters for these atoms, thus requiring further approximations. In earlier studies, neutron diffraction was extensively used to obtain independent thermal parameters. But this method is hampered by differences in systematic errors between the X-ray and neutron experiments, which are not fully understood. An elegant solution has been developed by Koritsanszky (1998). Thermal amplitudes due to internal molecular modes can now be obtained (in the harmonic approximation) for small molecules with standard theoretical software packages. Once these are introduced, the remainder of the molecular motion can be treated as the motion of a rigid body, or an assembly of rigid bodies. For DL-aspartic acid (Flaig *et al.*, 1998), this method has been shown to be remarkably successful. It reduces the number of parameters while giving physically more reliable results.

There are indications that for very precise low-temperature data the formalism (1) may not be sufficiently flexible. Additional functions that allow for radial migration of the density may be needed. Furthermore, the radial functions may depend not only on the index l but also on m, and for very high resolution data small deformations of the core density may become visible. This may be the next inner shell, such as the L shell of silicon or the innermost electrons. For the inner shells, deformations have been predicted on the basis of the electrostatic Hellmann–Feynman theorem, which states that electrostatic forces on the nuclei must vanish at equilibrium. As shown by Hirshfeld (Hirshfeld & Rzotkiewicz, 1974), in order to achieve a balance, the core electrons undergo a slight, but sharp, polarization that opposes the field exerted by the valence electrons.

4. The features of aspherical atoms

What are the features of the aspherical pseudoatoms and to what extent are they transferable between chemically similar sites? Not unexpectedly, their shape depends very much on the symmetry of the bonding environment. The trigonal environment of an sp^2-hybridized C atom or the tetrahedral environment of an sp^3-hybridized atom is well represented by the octupolar ($l = 3$) spherical harmonic density functions, such as (without normalization) $x^3 - 3xy^2$ and xyz (Coppens,

1997). The deformation of a terminal H atom, or of an acetylenic C atom, requires dipolar functions, and those are indeed found to be occupied prominently by the least-squares refinement of good-quality data sets. For atoms with lone-pair electrons, the deformation depends very much on the arrangement of the lone-pair orbitals and their relation to the bonds. Such regularities are best analyzed with a set of related molecules. Arguing that charge-density analysis of ever larger molecules, and in particular well diffracting macromolecules, requires a standard set of aspherical-atom form factors, Lecomte and co-workers are composing a database of aspherical atoms (Pichon-Pesme *et al.*, 1995). Using the experimental densities on a number of amino acids and oligopeptides, they have averaged the aspherical features to obtain a standard set. Results for a section through sp^2- and sp^3-hybridized carbon atoms are shown in Fig. 3. When such atoms are used to analyze low-
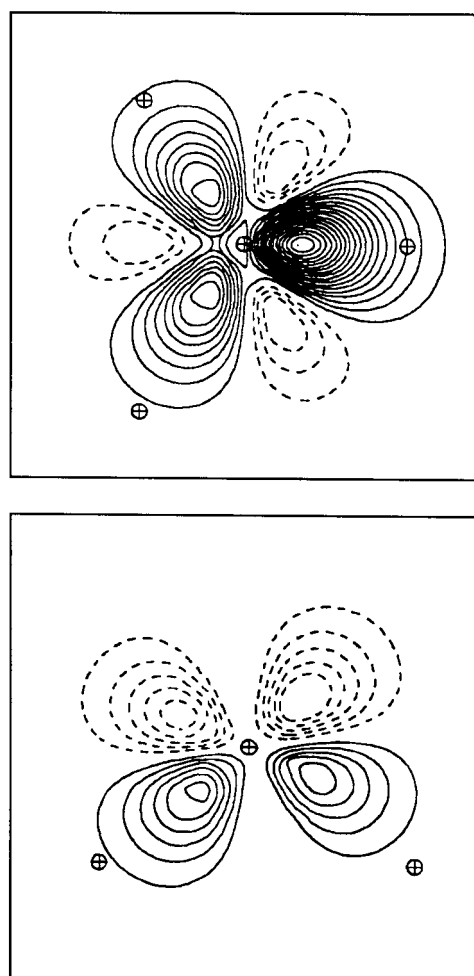

Fig. 3. Sections through the static deformation densities for an sp^2 (top) and an sp^3 (bottom) C atom as determined by least-squares refinement based on the aspherical-atom formalism. Contour interval 0.05 e Å^{-3}. Negative contours dashed, zero contour omitted. From Pichon-Pesme *et al.* (1995).

Table 1. *Experimental d-electron populations in low-spin bispyridine (meso-phenyl porphinato)iron(II) (A) (Li et al., 1988) and in high-spin bis(tetrahydrofuran) (meso-tetraphenylporphinato)iron(II) (B) (Lecomte et al., 1986)*

Orbital	A		B	
$d_{x^2-y^2}$	0.35	4.8%	1.42	24.0%
d_{z^2}	1.05	14.4%	1.04	17.5%
$d_{xz,yz}$	3.86	53.0%	2.52	42.6%
d_{xy}	2.02	27.7%	0.93	15.7%

resolution data, an improvement in the R factors is observed and the rigid-bond test is more closely obeyed. The standard atoms can form the basis for a further refinement including valence populations and net atomic charges and be used in future analyses of the electrostatic interactions in macromolecules.

For transition-metal atoms, the aspherical nature of the atoms is dominated not so much by the covalent bonds but by the preferential occupancy of the d orbitals in the field exerted by the ligands. In low-spin complexes in particular, the asymmetry can be pronounced. For a d^6 Fe^{2+} atom in a strong octahedral field, for example, the t_{2g} orbitals, which point into the voids between the bonds, will be fully occupied, while the e_g orbitals, pointing towards the ligands, are populated only through σ donation from the ligand atoms. The difference between low-spin and high-spin Fe^{2+} deformation-density maps is illustrated in Fig. 4. Because of the low contribution from covalency, the d-orbital populations of the metal atom can be estimated from the population coefficients as determined with the multipole formalism (Holladay *et al.*, 1983). The populations corresponding to the maps in Fig. 4 are given in Table 1.

5. Electrostatic moments

A remarkably good dipole moment for uracil was obtained from X-ray data by Stewart in 1970 (Stewart, 1970). Since then, a large number of molecular dipole and quadrupole moments have been obtained, either by direct integration of the electron density or from the population parameters and density functions of the least-squares refinement. The results up to 1992 have been summarized by Spackman (1992). It should be noted that X-ray diffraction does not yield highly accurate electrostatic moments, but the method is generally applicable and yields solid-state rather than gas- or liquid-phase moments. Unlike dielectric measurement of dipole moments, X-ray diffraction provides not only the magnitude but also the orientation of the moments.

Not unexpectedly, the moments for a molecule in a solid are generally larger than those calculated theoretically for isolated molecules, in agreement with recent theoretical results for molecules in solution (Gao & Xia, 1992; Gao, 1996). For small molecules with conjugated double bonds in polar solvents, dipole-moment enhancements can be pronounced (Gao, 1997).

In crystals, the enhancement will be both a function of the polarizability of the molecule and of the packing arrangement. The water molecule has a dipole moment of 1.84 D in the gas phase while reported X-ray values cluster around 2.25 D. For comparison, a theoretical calculation gives 2.23–2.73 D for ice VIII and a number of prototype structures (Gatti *et al.*, 1995). However, theoretical dipole moments are quite basis-set dependent and are affected by electron correlation.
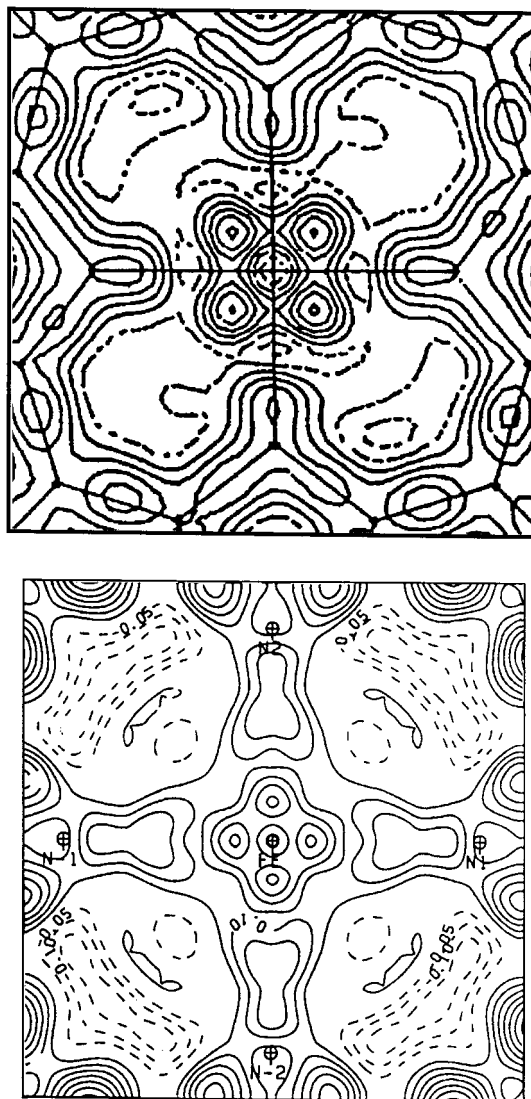

Fig. 4. Deformation density in two different Fe porphyrins in the plane containing the Fe atom and the porphyrin ring. Top: low-spin Fe^{II}(pyridine)$_2$ tetraphenylporphyrin. Bottom: high-spin Fe^{II}(tetrahydrofuran)$_2$ tetraphenylporphyrin. Contours at 0.05 e Å^{-3}. From Li *et al.* (1988) and Lecomte *et al.* (1986).

Table 2. *Comparison of topological parameters for three types of bonds in a number of amino acids (Abramov, Koritsanszky & Coppens, 1998)*

R: bond length; ρ_b: density at the bond critical point; $\nabla^2\rho_b$: the Laplacian at the bond critical point; $\lambda_1, \lambda_2, \lambda_3$: principal components of $\nabla^2\rho_b$; ε: ellipticity of the bond; n: bond order, as derived from ρ_b.

Bond	Compound	R (Å)	ρ_b (e Å^{-3})	ε	λ_1 (e Å^{-5})	λ_2 (e Å^{-5})	λ_3 (e Å^{-5})	$\nabla^2\rho_b$ (e Å^{-5})
C1—O2	DL-Histidine	1.265	2.66	0.08	−23.5	−21.9	11.2	−34.2
	DL-Aspartic acid	1.255	2.87	0.29	−28.8	−22.4	15.1	−36.1
	DL-Proline	1.268	2.83	0.16	−29.5	−25.3	14.3	−40.5
	L-Dopa	1.260	2.64	0.25	−28.2	−22.6	12.1	−38.8
	L-Alanine	1.267	2.86	0.13	−27.6	−24.4	22.5	−29.5
C2—N1	DL-Histidine	1.483	1.61	0.45	−10.3	−7.1	10.1	−7.3
	DL-Aspartic acid	1.491	1.69	0.09	−13.0	−11.9	12.0	−12.9
	DL-Proline	1.504	1.67	0.19	−13.6	−11.4	15.1	−9.8
	L-Dopa	1.495	1.62	0.47	−12.7	−8.6	12.9	−8.4
	L-Alanine	1.488	1.70	0.30	−13.9	−10.7	13.6	−11.0
C1—C2	DL-Histidine	1.539	1.73	0.21	−12.1	−10.0	8.8	−13.2
	DL-Aspartic acid	1.537	1.69	0.25	−13.7	−10.9	11.7	−12.9
	DL-Proline	1.529	1.88	0.20	−15.4	−12.8	13.0	−15.2
	L-Dopa	1.536	1.71	0.14	−12.5	−11.0	11.4	−12.0
	L-Alanine	1.535	1.76	0.21	−13.5	−11.2	13.8	−10.9

References to data: DL-histidine, Coppens *et al.* (1998); DL-aspartic acid, Flaig *et al.* (1998); DL-proline, Koritsanszky *et al.* (1998); L-dopa, Howard *et al.* (1995); L-alanine, Destro *et al.* (1989).

An extensive theoretical study on the molecule of urea and its crystals (Gatti *et al.*, 1994) sheds further light on the effect of crystal packing. According to the calculation, in the crystal the molecular dipole moment is increased from 5.15 D for the isolated molecule, to 7.04 D. It is found that the H atoms become more positive and the other atoms more negative, or less positive, upon crystallization, thus accounting for the increase in dipole moment. The sublimation energy of the crystal is reproduced within experimental limits by the calculation.

For somewhat larger molecules, such as amino acids, the matrix effects tend to increase when the molecule contains conjugated bonds or aromatic rings. For example, for L-alanine and DL-proline, the X-ray values of 12.9 and 13.0 D, respectively, are close to the theoretical isolated molecule results of 12.4 (Destro *et al.*, 1989) and 12.6 D (Koritsanszky *et al.*, 1998), respectively. But for the histidine molecule in crystals of DL-histidine, the difference is larger, with X-ray and isolated molecule values of 17.4 and 15.9 D, respectively (Carducci *et al.*, 1997). This is as expected on the basis of polarizability arguments.

The number of amino acids and peptides studied accurately is still rather small and parallel theoretical calculations on clusters and solids are still rare. Nevertheless, the environment-induced changes in the charge distribution are of crucial importance. It has become clear that induced polarization due to inter- and intramolecular interactions must be understood for the derivation of reliable force fields, which are needed in the analysis of protein folding (Beachy *et al.*, 1997). The combination of theory and experiment is expected to yield the required information.

6. Topological analysis and experimental charge densities

6.1. *The relation between the topology of the density and chemical concepts*

The theory of *atoms in molecules* (AIM) of Bader and co-workers (Bader, 1990) quantifies the interactions between atoms in terms of the topology of the total electron density and its Laplacian, $\nabla^2\rho$. The electron density is, in Bader's words, '*a physical manifestation of the forces acting within the system*', and thus a detailed source of information on that system. The dominant topological feature of the charge density is the occurrence of local maxima at the positions of the nuclei as a consequence of the attractive forces between the electrons and the nuclei. The maxima are *critical points* at which the first derivatives of the density are zero and the
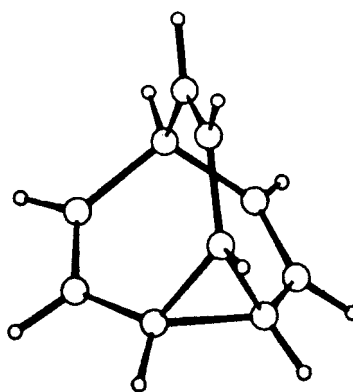

Fig. 5. The molecule of bullvalene. Large circles: C atoms; small circles: H atoms.

curvature of the electron density is negative in all directions. Other critical points with zero first derivatives, but different sign of the curvatures, occur at the saddle points of the density in bonds between atoms, at the center of rings of atoms and at local minima. The critical points are labeled with a 3, for three dimensions, and a second number which is the sum of the signs of the curvatures at the point. Thus, the critical point at the position of an atom is a $(3, -3)$ critical point. A bond is defined by the *bond path*, which is the line of maximum density linking two atoms. The bond path deviates from the line connecting two atoms when the bond is bent; the distance from the $(3, -1)$ critical point to the line connecting the atoms is a measure of the degree of bending of the bond.

The theory relates bond order to the electron density at the bond critical point and the nature of the bonding interaction to several topological parameters. The foremost of these is the value of the Laplacian at the bond critical point. In a covalent bond, the density is contracted in the plane through the critical point perpendicular to the bonding direction. This contraction manifests itself in the negative principal values, λ_1 and λ_2, of the curvatures in this plane. If the contraction outweighs the positive curvature along the bond paths, the Laplacian at the $(3, -1)$ critical point is negative and the interaction is defined as a *shared interaction*. If it is positive, it is defined as a *closed-shell interaction*.† The quantity $\lambda_1/\lambda_2 - 1$ is defined as the *ellipticity* of the bond, which is an indication of double-bond character. The polarity of the bond can be gauged from the deviation of the critical point from the midpoint of the bond path.

6.2. *Experimental densities and topological analysis*

Since the AIM theory uses the charge density as its central concept, it is an ideal match for experimental charge-density analysis. As noted above, the experimental 'model density' is in principle a static density. In the Born–Oppenheimer approximation, this 'static density' will be an average over the static densities of each of the points along the vibrational surface of the molecule or crystal, which is not the same as the hypothetical stationary density calculated by quantum-mechanical methods. Cooling to the lowest possible experimental temperature should minimize any such differences.

A pioneering first systematic topological analysis using both experimental and theoretical results was published in 1992 by Gatti *et al.*, based on experimental data on L-alanine collected at 23 K. The agreement between theory and experiment for the non-polar C—C

bonds is excellent. But for C—O and C—N bonds discrepancies in the value of the Laplacian $\nabla^2\rho$ and the location of the critical point exist, which, though reduced by extension of the theoretical basis set, remain considerable. As shown in a later study of DL-histidine, for example, the experimental values for the Laplacian and its components at the critical points of the C—O and C—N bonds do not agree with Hartree–Fock theory
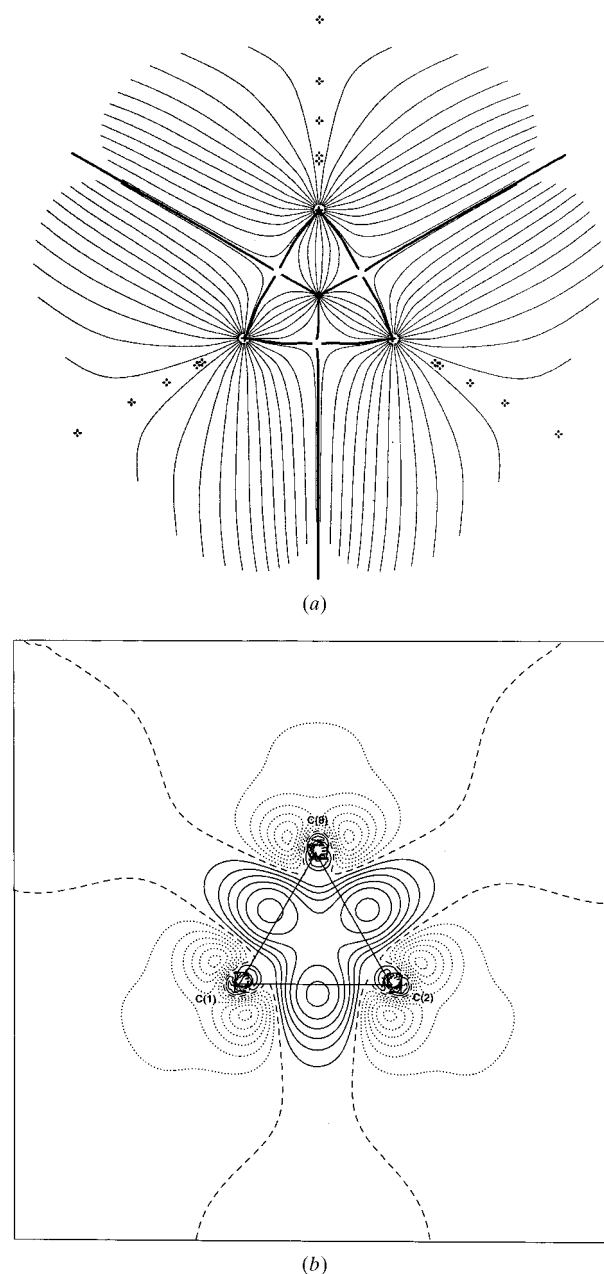

(a)

(b)

Fig. 6. (a) Map of the gradient vector field of the theoretical charge density in the cyclopropane ring of bullvalene. The bond paths connecting the atoms and lines denoting the interatomic surfaces in this plane are drawn as heavy lines. (b) Experimental deformation density in this plane. From Koritsanszky *et al.* (1996).

† This classification may need some revision for bonds involving second- and higher-row atoms, for which the positive value of λ_3 is large and may not outweigh the contraction into the bond, even if the latter is considerable.

Table 3. *Topological parameters for the bonds in bullvalene*

Units and symbols as in Table 2 (Koritsanszky *et al.*, 1996).

Bond	C═C	$C(ring)$─C	C─C	$C(ring)$─$C(ring)$
ρ_b	2.36 (2)	1.92 (2)	1.78 (1)	1.54 (1)
$\nabla^2\rho_b$	−26.0 (1)	−19.3 (1)	−16.0 (1)	−7.3 (1)
ε	0.29	0.09	0.04	0.90
n	2.09	1.33	1.11	0.89

even at the 6-311G**(3*d*, 3*f*) level, but they do agree quite well with experimental values for comparable bonds in DL-proline, DL-aspartic acid, L-DOPA and L-alanine (Table 2) (Abramov, Koritsanszky & Coppens, 1998). The analysis of Gatti *et al.* (1992) shows that the Laplacian values along the path of polar bonds, and the exact location of the bond critical points are very much affected by electron correlation, which implicitly is included in the experimental results.

An example of a topological analysis of a complex hydrocarbon is the study on bullvalene (tricyclo[3.3.2.0$^{2.8}$]deca-3,6,9-triene), a trigonal 'tent-shaped' molecule with a three-membered cyclopropane ring at its base (Fig. 5) (Koritsanszky *et al.*, 1996). The topological parameters clearly distinguish between the different C─C bonds in terms of bond order, ellipticity and value of the Laplacian at the bond critical point (Table 3). The ellipticity ε is a very good indication of the deviation from cylindrical symmetry of the bond. Such deviations were quite evident in early deformation-electron-density maps but are not as easily quantified from such maps. In bullvalene, the ring bonds are weaker than the other C─C bonds but have a very large ellipticity owing to the contraction of the density into the plane of the three-membered ring. As observed in other cyclic ring systems, the bond paths in the ring are bent outward (Fig. 6*a*), the bond critical point being displaced by 0.02 Å from the line connecting the C atoms. Interestingly, the maximum of the bond peak in the deformation density is displaced much further outwards, by 0.12 Å, an indication of the sensitivity of the deformation density to certain bonding features (Fig. 6*b*).

In 1964, in an often overlooked paper, Hirshfeld described how examination of the geometry of a series of compounds of the type RXR' leads to the conclusion that the bonding hybrid orbitals in such molecules make smaller angles with each other than the internuclear vectors (Hirshfeld, 1964). The cause of the effect is repulsion between non-bonded atoms two bonds apart. In other words, such bonds are bent *inwards*. In dimethyl ether, CH_3OCH_3, for example, the threefold axes of the CH_3 groups do not coincide with the O─C bonds. Direct charge-density evidence for the effect was obtained for several molecules (Eisenstein & Hirshfeld, 1979) and more recently from both the deformation density and from topological analysis of the total density of the ammonia molecule (Boese *et al.*, 1997). Such studies on substances that are gases at ambient temperature require very careful experimentation but have been performed only in a few cases (Stevens, 1979). As in bullvalene, for NH_3 the effect is more pronounced in the DED, in which the maximum is shifted by 0.15 Å from the internuclear line, while the experimental N─H bond critical point is displaced by only 0.02 Å.

At this time, the topological analysis of transition-metal complexes is relatively unexplored. But the possibilities for such studies are numerous. In a recent study, Macchi *et al.* (1998) show how the topology of the bond paths between the metal atom and an η^2-coordinated ligand depends on the nature of the interaction (Fig. 7). In bis(1,5-cyclooctadiene)nickel, the bond paths are slightly curved inward but separate (Fig. 7, rightmost diagram), a pattern typical for both π back-donation and σ donation. In contrast, in a nickel complex studied by Smith *et al.* (1997), a single bond path emanates from the Ni atom towards three liganded OH groups and then divides into separate branches to each of the ligand atoms.

The new topological analyses complement earlier seminal studies of metal–ligand bonding based on the deformation density, initiated by Rees & Mitschler (1976) on $Cr(CO)_6$.

A combined X-ray and neutron diffraction study of the metal hydride *cis*-[$Mn(CO)_4HPPh_3$] by Brammer and co-workers gives direct evidence for a bond path connecting the hydride H atom and a phenyl H atom
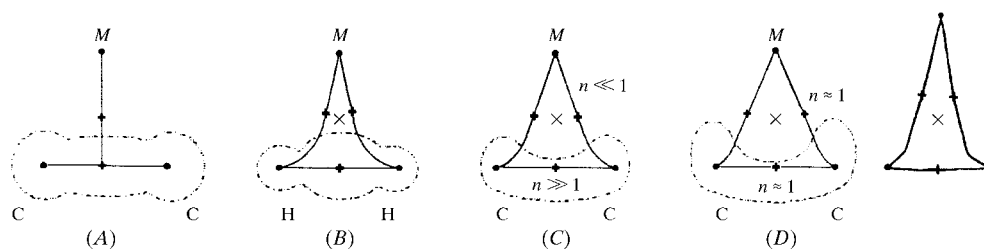

Fig. 7. Schematic bond-path geometries for different types of bihapto metal–ligand bonding. (*A*): ionic interaction with a π ligand. (*B*): σ donation into a σ bond plus back-donation into a σ^* ligand orbital, such as occurs for side-bound H_2. (*C*): σ donation into a π bond plus back-donation into a π^* ligand orbital according to the Dewar–Chatt model. (*D*): metallacycle with the presence of two covalent M─C interactions. The diagram on the far right is the experimental result for bis(1,5-cyclooctadiene)nickel. From Macchi *et al.* (1998).

(Abramov, Brammer, Klooster & Bullock, 1998). Together with the negative charge on the hydrogen of ~ -0.4 e, this constitutes the most direct evidence yet for the unusual $M-\text{H}\cdots\text{H}-\text{C}$ interaction

7. Charge-density analysis of intermolecular interactions

As the X-ray technique yields the crystal, rather than the isolated-molecule or cluster-of-molecules density, it is not surprising that there is a renewed interest in experimental density studies of intermolecular interactions. Hydrogen bonds are of course among the foremost of such interactions. Experimental and theoretical work by Feil and Hermansson and their collaborators (Krijn *et al.*, 1988; Hermansson, 1985) indicates a depletion of density at the H atom and an enhancement of the density in the $X-\text{H}$ bond. The effect in the lone-pair region of the acceptor atom of the H bond is more complex. For the longer bonds, there is a depletion of density in this region but the effect is reversed for short strong hydrogen bonds. The H-bond interaction can be considered a combination of attractive Coulombic forces and exchange repulsion between the density of the proximal atoms. In the short bonds, the former causes an enhancement of the lone-pair density. This is evident in the many experimental studies on α-oxalic acid (Coppens *et al.*, 1984) in which one of the $O-\text{H}\cdots\text{O}$ bonds has an $O\cdots O$ distance of 2.524 Å (Coppens & Sabine, 1969). But, as Feil has shown, in longer bonds this polarization of the lone-pair density is masked by the exchange repulsion (Feil, 1995).

The topological analysis generally shows a contraction in the plane through the critical point perpendicular to the H-bond path. But the overall value of the Laplacian is positive at 2–5 e Å^{-5} for most $O-\text{H}\cdots\text{O}$ and $N-\text{H}\cdots\text{O}$ bonds (Destro *et al.*, 1989; Howard *et al.*, 1995; Flaig *et al.*, 1998), indicating formally a closed-shell interaction. As shown by Flensburg *et al.* (1995), very short H bonds are an exception. They have negative Laplacians at the bond critical point and show a pronounced contraction in the perpendicular plane.

Since $X-\text{H}\cdots Y$ interactions are ubiquitous in molecular crystals and responsible for much of the energy of stabilization of molecular crystals and macromolecules, their study has relevance in other fields. The increasing number of experimental charge densities have made it possible to compare the H-bond topological parameters with other quantities describing the H bond. Similarly, significant, though not always perfect, correlations have been established between the topological parameters of an H bond and its dissociation energy, as calculated theoretically (Boyd & Choi, 1985, 1986; Carroll & Bader, 1988; Popelier & Bader, 1992; Koch & Popelier, 1995). Espinosa *et al.* (1998) have analyzed the experimental densities of a number of oligopeptides, which are especially suitable for this purpose, since as a group they contain a large number of similar interactions. A func-

tional proposed by Abramov gives a relation between the topological parameters at the bond critical point and the kinetic energy density (Abramov, 1997), thus establishing a direct connection between density and energy values. Some of the results of the application of the functional by Espinosa *et al.* (1998) are presented in Fig. 8. Such work has considerable potential in future analysis of intermolecular interactions in crystals.

8. Concluding remarks

Only a very small fraction of the available charge-density studies have been mentioned in this article. During the past four decades, charge-density analysis has developed into a technique now ready for application to a broad range of problems of interest in chemistry, biology and solid-state physics. The field has matured and two texts are now available (Tsirelson & Ozerov, 1996; Coppens, 1997). The time may not be far off for on-line measurement and analysis of charge densities, perhaps using previously obtained structural information. New software packages, such as *XD*
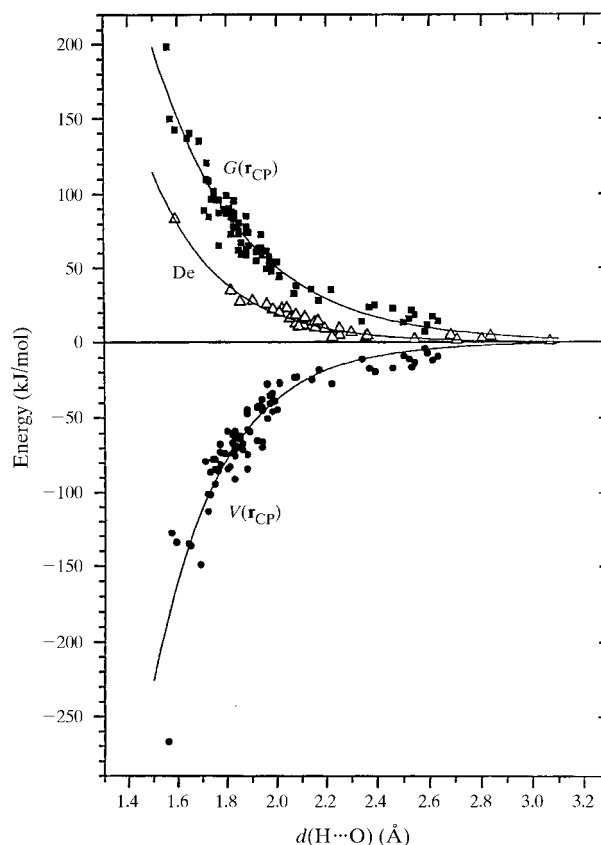
Fig. 8. Experimental kinetic energy density at the bond critical point $G(\mathbf{r}_{CP})$ [kJ (mol a.u.^{3})$^{-1}$], experimental potential energy density $V(\mathbf{r}_{CP})$ and theoretical dissociation energy (kJ mol^{-1}), as a function of the H$\cdots$O distance. From Espinosa *et al.* (1998).

(Koritsanszky *et al.*, 1997), are to play a major role in this development.

Frontier areas not mentioned above, that are actively being developed, are the derivation of the first-order density matrix from the diffraction data, combining analysis of charge densities with spin and momentum densities, and the study of the charge density of laser-induced molecular excited states. This is a large frontier, which, as the past has shown, will advance with further developments in methods, instrumentation and computing capability.

References

Abramov, Y. A. (1997). *Acta Cryst.* A**53**, 264–272.

Abramov, Y. A., Brammer, L., Klooster, W. T. & Bullock, R. M. (1998). Private communication.

Abramov, Y., Koritsanszky, T. & Coppens, P. (1998). To be published.

Bader, R. F. W. (1990). *Atoms in Molecules: a Quantum Theory.* Oxford: Clarendon Press, Oxford Science Publications.

Beachy, M. D., Chasman, D., Murphy, R. B., Halgren, T. A. & Friesner, R. A. (1997). *J. Am. Chem. Soc.* **119**, 5908–5920.

Boese, R., Niederprüm, N., Bläser, D., Maulitz, A., Antipin, M. Y. & Mallinson, P. R. (1997). *J. Phys. Chem.* **101**, 5794–5799.

Boyd, R. J. & Choi, S. C. (1985). *Chem. Phys. Lett.* **120**, 80–85.

Boyd, R. J. & Choi, S. C. (1986). *Chem. Phys. Lett.* **129**, 62–65.

Carducci, M., Pressprich, M. R. & Coppens, P. (1997). *J. Am. Chem. Soc.* **119**, 2669–2678.

Carroll, M. T. & Bader, R. F. W. (1988). *Mol. Phys.* **65**, 695–722.

Coppens, P. (1997). *X-ray Charge Densities and Chemical Bonding.* New York: Oxford University Press.

Coppens, P., Abramov, Y., Carducci, M., Korgov, B., Novozhilova, I. & Pressprich, M. (1998). To be published.

Coppens, P., Dam, J., Harkema, S., Feil, D., Feld, R., Lehmann, M. S., Goddard, R., Krüger, C., Hellner, E., Johansen, H., Larsen, F. K., Koetzle, T. F., McMullan, R. K., Maslen, E. N. & Stevens, E. D. (1984). *Acta Cryst.* A**40**, 184–195.

Coppens, P., Guru-Row, T. N., Leung, P., Becker, P. J., Yang, Y. W. & Stevens, E. D. (1979). *Acta Cryst.* A**35**, 63–72.

Coppens, P. & Sabine, T. M. (1969). *Acta Cryst.* B**25**, 2442–2451.

Destro, R., Bianchi, R. & Morosi, G. J. (1989). *J. Phys. Chem.* **93**, 4447–4457.

Eisenstein, M. & Hirshfeld, F. L. (1979). *Chem. Phys. Lett.* **42**, 465–474.

Espinosa, E., Molins, E. & Lecomte, C. (1998). *Chem. Phys. Lett.* **285**, 170–173.

Feil, D. (1995). Private communication.

Flaig, R., Koritsanszky, T., Zobel, D. & Luger, P. (1998). *J. Am. Chem. Soc.* **120**, 2227–2238.

Flensburg, C., Larsen, S. & Stewart, R. F. (1995). *J. Phys. Chem.* **99**, 10130–10141.

Gao, J. (1996). *Reviews in Computational Chemistry*, Vol. 7, edited by K. B. Lipkowitz & D. B. Boyd, p. 119. New York: VCH.

Gao, J. (1997). *J. Am. Chem. Soc.* **119**, 2962–2963.

Gao, J. & Xia, X. (1992). *Science*, **258**, 631–635.

Gatti, C., Bianchi, R., Destro, R. & Merati, F. (1992). *J. Mol. Struct. (Theochem.)*, **255**, 409–433.

Gatti, C., Saunders, V. R. & Roetti, C. (1994). *J. Chem. Phys.* **101**, 10686–10696.

Gatti, C., Silvi, B. & Colonna, F. (1995). *Chem. Phys. Lett.* **247**, 135–141.

Hansen, N. K. & Coppens, P. (1978). *Acta Cryst.* A**34**, 909–921.

Hermansson, K. (1985). *Acta Cryst.* B**41**, 161–169.

Hirshfeld, F. L. (1964). *Isr. J. Chem.* **2**, 87–90.

Hirshfeld, F. L. (1976). *Acta Cryst.* A**32**, 239–244.

Hirshfeld, F. L. & Rzotkiewicz, S. (1974). *Mol. Phys.* **27**, 1319–1343.

Holladay, A., Leung, P. C. & Coppens, P. (1983). *Acta Cryst.* A**39**, 377–387.

Howard, S. T., Hursthouse, M. B., Lehmann, C. W. & Poyner, E. A. (1995). *Acta Cryst.* B**51**, 328–337.

Irngartinger, H. (1982). *Electron Distributions and the Chemical Bond*, edited by P. Coppens & M. B. Hall, pp. 361–379. New York: Plenum Press.

Iversen, B. B., Larsen, F. K., Figgis, B. N., Reynolds, P. A. & Schultz, A. J. (1996). *Acta Cryst.* B**52**, 923–931.

Iversen, B. B., Larsen, F. K., Figgis, B. N. & Reynolds, P. A. (1997). *J. Chem. Soc. Dalton Trans.* pp. 2227–2240.

Koch, U. & Popelier, P. L. A. (1995). *J. Phys. Chem.* **99**, 9747–9754.

Koritsanszky, T. (1998). *Acta Cryst.* In preparation.

Koritsanszky, T., Buschmann, J. & Luger, P. (1996). *J. Phys. Chem.* **100**, 10547–10553.

Koritsanszky, T., Flaig, R., Zobel, D., Krane, H.-G., Morgenroth, W. & Luger, P. (1998). *Science*, **279**, 356–358.

Koritsanszky, T., Howard, S. T., Su, Z., Mallinson, P. R., Richter, T. & Hansen, N. K. (1997). *XD, Computer Program Package for Multipole Refinement and Analysis of Electron Densities from Diffraction Data.* Free University of Berlin, Germany.

Krijn, M. P. C. M., Graafsma, H. & Feil, D. (1988). *Acta Cryst.* B**44**, 609–616.

Larsen, F. K. (1995). *Acta Cryst.* B**51**, 468–482.

Lecomte, C., Blessing, R. H., Coppens, P. & Tabard, A. (1986). *J. Am. Chem. Soc.* **108**, 6942–6950.

Li, N., Coppens, P. & Landrum, J. (1988). *Inorg. Chem.* **27**, 482–488.

Macchi, P., Proserpio, D. M. & Sironi, A. (1998). *J. Am. Chem. Soc.* **120**, 1447–1455.

Pichon-Pesme, V., Lecomte, C. & Lachekar, H. (1995). *J. Phys. Chem.* **99**, 6242–6250.

Popelier, P. L. A. & Bader, R. F. W. (1992). *Chem. Phys. Lett.* **189**(6), 542–548.

Rees, B. & Mitschler, A. (1976). *J. Am. Chem. Soc.* **98**, 7918–7924.

Smith, G. T., Mallinson, P. R., Frampton, C. S., Farrugia, L. J., Peacock, R. D & Howard, J. A. K. (1997). *J. Am. Chem. Soc.* **119**, 5028–5034.

Spackman, M. A. (1992). *Chem. Rev.* **92**, 1769–1797.

Stevens, E. D. (1979). *Mol. Phys.* **37**(1), 27–45.

Stewart, R. F. (1970). *J. Chem. Phys.* **53**, 205–213.

Stewart, R. F. (1976). *Acta Cryst.* A**32**, 565–574.

Tsirelson, V. G. & Ozerov, R. P. (1996). *Electron Density and Bonding in Crystals.* Bristol, England/Philadelphia, PA: Institute of Physics Publishing.